Atmos. Meas. Tech. Discuss., https://doi.org/10.5194/amt-2019-51
Manuscript under review for journal Atmos. Meas. Tech.
Discussion started: 17 April 2019

Atmospheric Measurement Techniques
Discussions

Estimating raindrop size distributions using microwave link measurements

Thomas C. van Leth[1], Hidde Leijnse[2], Aart Overeem[1,2], and Remko Uijlenhoet[1]

[1]Hydrology and Quantitative Water Management Group, Wageningen University
[2]R&D Observations and Data Technology, Royal Netherlands Meteorological Institute (KNMI)

Correspondence to: Thomas C. van Leth (tommy.vanleth@wur.nl)

Abstract. We present a novel method of using two or three collocated microwave link instruments to estimate the three parameters of a gamma raindrop size distribution (DSD) model. This allows path-average DSD measurements over a path length of several kilometers as opposed to the point measurements of conventional disdrometers. Our method is validated in a round-trip manner using simulated DSD fields as well as five laser disdrometers installed along a path. Different potential link combinations of frequency and polarization are investigated. We also present preliminary results from the application of this method to an experimental setup of collocated microwave links measuring at 26 GHz and 38 GHz along a 2.2 km path. Simulations show that a DSD retrieval on the basis of microwave links can be highly accurate. We found that a triple link retrieval provides no added benefit over a dual link retrieval. In practice, the accuracy and success of the retrieval is highly dependent on the stability of the base power level.

1 Introduction

The use of microwave links to measure rainfall intensity has received significant attention in the last decade. The main driver for this has been the insight that the backhaul links of mobile communication networks are suitable for such measurements and are available in greater numbers than dedicated rainfall measurement stations in many countries (Messer et al., 2006; Leijnse et al., 2007b; Gosset et al., 2016). In addition, efforts have been taken to expand the range of atmospheric phenomena that can be measured with microwave links including fog (David et al., 2013), solid precipitation (Cherkassky et al., 2014) and evapotranspiration (Leijnse et al., 2007a). Another enticing possibility is the use of multiple link instruments along the same path to measure not just the bulk rainfall intensity, but the path-average raindrop size distribution (DSD).

DSD estimates can be used to derive all other bulk rainfall variables and are therefore valuable for a variety of purposes (see e.g. Uijlenhoet and Stricker (1999) for an overview of relevant statistical moments). Examples include precipitation microphysics (e.g. Uijlenhoet et al. (2003)), soil erosion by rain (e.g. Angulo-Martínez and Barros (2015); Salles et al. (1999); Salles and Poesen (1999, 2000)) and radar validation (e.g. Hazenberg et al. (2014)). The use of microwave links for such purposes promises measurements that are more spatially representative of radar or satellite pixels than what is offered by the usually sparse networks of impact, laser and video disdrometers that are currently the most common way DSDs are measured.

In order to estimate the DSD from a limited number of statistical moments, a parameterization has to be used. The gamma distribution with three parameters provides a good estimate for a wide variety of rainfall events (Ulbrich, 1983). Rincon and Lang (2002) where first to attempt a gamma DSD parameter retrieval using two microwave links with promising results. However, their methods require an a priori parameter estimate in addition to the parameters derived from the two measurements. To the best of our knowledge, no further research has been published regarding DSD estimations using microwave links. However, the adjacent field of polarimetric radar measurement has seen much development (see e.g. Fabry (2015)) and many different methods to estimate DSDs from polarimetric radar have now been developed and tested.

A handful of different techniques can be identified that have been developed to retrieve DSD parameters from a limited number of polarimetric radar moments: The constrained gamma method developed by Zhang et al. (2001), the β method proposed by Gorgucci et al. (2002) and double-moment DSD normalization (Raupach and Berne, 2017). Several machine learning approaches have also been used: neural networks (Vulpiani et al., 2006), Bayesian regression (Cao et al., 2010) and tree-based genetic programming (Islam et al., 2012).

In this paper we will explore the potential of a numerical retrieval from microwave attenuation and/or differential propagation phase shift. We consider two different techniques: The first method uses three measured microwave link variables to derive the three parameters of the gamma distribution. Here the gamma parameters are weakly constrained (i.e., only a limited range of parameter values is allowed). The other method uses two measured microwave link variables to derive two parameters of the gamma distribution. Here, the third parameter is completely constrained by the other two, similar to the method used by Zhang et al. (2001) for radar moments. We will apply these techniques first using a simulated dataset based on radar and disdrometer measurements from the Ardèche region, France. Next, we will apply the method to microwave link variables derived from a set of path-averaged measurements from five laser disdrometers in Wageningen, The Netherlands. Finally, we will test the methods on measurements from microwave link instruments along the same path as the disdrometers in Wageningen (Van Leth et al., 2018) and compare the resulting DSDs with the DSDs measured from the disdrometers.

The paper is organized as follows: In Section 2 we present in more detail the datasets used in this paper. In Section 3 we present the theory and the methods used to retrieve DSDs from microwave link variables. We will also describe the validation methods employed. In Section 4 we discuss the results retrieved from the Ardèche dataset. In Section 5 we discuss the results of several tests using simulated attenuations from the Wageningen disdrometer dataset. We also consider the efficacy of different frequency combinations and the robustness of the retrieval to measurement uncertainty. In Section 6 we will apply the developed methods to actual link measurements that were obtained in Wageningen. In Section 7 we will present our thoughts on the feasibility of the techniques in practice and the choices made in this paper. Finally, in Section 8 we come to conclusions and give recommendations for further study.

Atmos. Meas. Tech. Discuss., https://doi.org/10.5194/amt-2019-51
Manuscript under review for journal Atmos. Meas. Tech.
Discussion started: 17 April 2019

Atmospheric Measurement Techniques Discussions

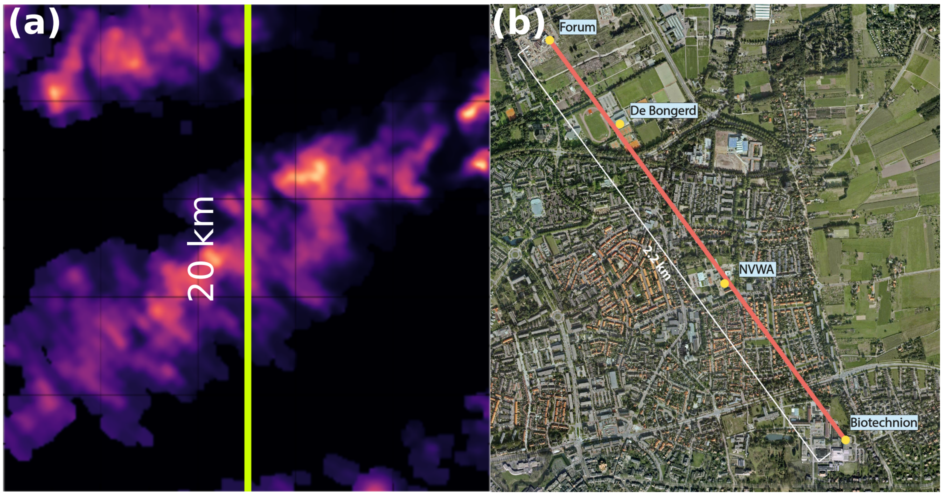

Figure 1. a) Sample rain field from the Ardèche dataset with the chosen transect. b) Positions of the disdrometers and the link path in the Wageningen dataset.

2 Data

2.1 Ardèche DSD reanalyses

Our first test-case consists of a 2-dimensional interpolated DSD field based on polarimetric radar data as well as disdrometer data measured in the Ardèche, France as part of the HyMeX campaign (Raupach and Berne, 2016). This field was generated using an advection-based temporal interpolation technique (Raupach and Berne, 2017). The data used here is based on a slightly improved version of that technique and was introduced by De Vos et al. (2018). This field has spatial dimensions of 20×20 km and a resolution of 100 m. It covers two distinct events on 27 November 2012 and 27 October 2013. Their durations are in the order of several hours and the time step is 30 s. The DSD is divided in 20 diameter bins with unequal bin width based on the detection bins of the OTT Parsivel^2 laser disdrometer measurements upon which the reanalysis is partially based. The smallest drop diameter class is 0.3 mm, while the largest diameter is 6.5 mm.

We take a transect through this field over the entire length of the field (Fig. 1a) and average the DSD over this transect to approximate the footprint of a microwave link. We calculate the attenuations and differential phase shifts for a number of frequencies: 15 GHz, 26 GHz, 32 GHz and 38 GHz. This includes the frequencies employed in the Wageningen experiment (see below) and covers the range of most commonly employed carrier frequencies in mobile phone networks.

In order to calculate the microwave link variables from the DSD data we first need to interpolate the data in the diameter dimension from the irregular bins to a regular diameter grid with a resolution of 0.1 mm. The main reason for this is to accurately reproduce the shape of the scattering cross sections as a function of diameter, as simply assuming the scattering cross section to be constant for the entire dD interval would introduce too much error. We have used a simple linear interpolation method for this purpose.

Atmos. Meas. Tech. Discuss., https://doi.org/10.5194/amt-2019-51
Manuscript under review for journal Atmos. Meas. Tech.
Discussion started: 17 April 2019

Atmospheric Measurement Techniques Discussions

2.2 Wageningen link experiment

Our second second test case is a microwave link experimental setup in Wageningen, The Netherlands (Van Leth et al., 2018). The setup consists of three collocated microwave links arranged between two buildings 2.2 km apart and covering mostly built-up terrain. The setup contains one dual-polarization 38 GHz link, which also measures the phase difference between the two polarizations, one additional single polarization 38 GHz link (not used for this paper) and a single polarization 26 GHz link. In addition five OTT Parsivel laser disdrometers are positioned at four locations beneath the link path, including the sites of the transmitting and receiving antennas, as shown in Fig. 1b. The data used in the following analyses is all taken from the period between 1 April 2015 and 1 January 2016. We also specifically focus on one event on 27 July 2015 for illustrative purposes.

In order to use the disdrometer data to represent the DSD of the link path we take a weighted spatial average over the disdrometer data. As with the Ardèche data, we interpolate the DSD data in the diameter dimension from the irregular bins to regular intervals before calculating the microwave link variables. In order to improve the robustness of the results, we only consider measurement intervals where each one of the five disdrometers counted at least 50 drops (see Uijlenhoet et al. (2006) on the effect of drop sample size on the robustness of the DSD estimate). We also apply the correction method of Raupach and Berne (2015) to the disdrometer DSDs.

3 Methods

3.1 Basic procedure

To determine the underlying DSD from a limited number of statistical moments we need an approximation with a limited number of parameters. One of the most widely used approximations for rain DSD is the gamma distribution suggested by Ulbrich (1983),

$$N(D) = N_0 D^{\mu} e^{-\Lambda D}, \tag{1}$$

where D is the drop diameter in mm, and N_0, μ and Λ are the parameters determining the shape and drop concentration. The parameter μ is a dimensionless shape parameter and Λ is a slope parameter with a unit of mm^{-1}. Note that the dimension of N_0 is dependent on the value of μ. Therefore it is convenient to also use a derived parameter,

$$N_T = N_0 \Lambda^{-(\mu+1)} \Gamma(\mu+1), \tag{2}$$

where Γ is the gamma function. N_T has the unit m^{-3} and is equal to the total drop concentration (assuming integration limits of 0 to ∞), resulting in

$$N(D) = N_T \frac{\Lambda}{\Gamma(\mu+1)} (\Lambda D)^{\mu} e^{-\Lambda D}. \tag{3}$$

Atmos. Meas. Tech. Discuss., https://doi.org/10.5194/amt-2019-51
Manuscript under review for journal Atmos. Meas. Tech.
Discussion started: 17 April 2019

Atmospheric Measurement Techniques
Discussions

The specific attenuation of a link signal in $\mathrm{dB\,km^{-1}}$ at a given frequency can be described in terms of the DSD,

$$k_H(\lambda) = C_k \frac{\lambda^2}{\pi} \int_0^\infty \Im[S_{HH}(\lambda, D)] N(D) dD \tag{4}$$

$$k_V(\lambda) = C_k \frac{\lambda^2}{\pi} \int_0^\infty \Im[S_{VV}(\lambda, D)] N(D) dD, \tag{5}$$

where λ is the wavelength of the incoming and outgoing waves in mm, $\Im$ is an operator indicating the imaginary part of its argument and $C_k = 10^{-3} \ln(10)^{-1}\ \mathrm{dB\,m^3\,km^{-1}\,mm^{-2}}$ is a unit conversion factor. S_{HH} and S_{VV} (dimensionless) are the diagonal components of the forward scattering amplitude matrix $\mathbf{S}$ defined by the relationship

$$\boldsymbol{E} = \mathbf{S} \cdot \boldsymbol{E_0}, \tag{6}$$

where $\boldsymbol{E_0}$ is the electric field strength of the incoming electromagnetic (EM) wave and $\boldsymbol{E}$ is the electric field strength of the outgoing EM wave. The specific phase shift (in $\mathrm{rad\,km^{-1}}$) between the horizontal and vertical components of an outgoing EM wave of a given frequency due to forward scattering can also be described as an integral over the DSD,

$$\phi(\lambda) = C_\phi \frac{\lambda^2}{\pi} \int_0^\infty \Re[S_{HH}(\lambda, D) - S_{VV}(\lambda, D)] N(D) dD, \tag{7}$$

where $\Re$ is an operator indicating the real parts instead of the imaginary parts of the diagonal components of the scattering amplitude matrix. $C_\phi = 10^{-3}\ \mathrm{m^3\,km^{-1}\,mm^{-2}}$ is another unit conversion factor.

The scattering efficiencies are defined as

$$Q_H(\lambda, D) = \frac{4\lambda^2}{\pi^2 D^2} \Im[S_{HH}(\lambda, D)] \tag{8}$$

$$Q_V(\lambda, D) = \frac{4\lambda^2}{\pi^2 D^2} \Im[S_{VV}(\lambda, D)] \tag{9}$$

$$Q_\phi(\lambda, D) = \frac{4\lambda^2}{\pi^2 D^2} \Re[S_{HH}(\lambda, D) - S_{VV}(\lambda, D)]. \tag{10}$$

It is the subtle differences in the shapes of the scattering efficiencies as functions of diameter for different frequencies and polarizations that contain the information necessary to retrieve the DSD. We calculate the scattering amplitude matrix using the T-matrix method (Waterman, 1965) following the approach of Mishchenko et al. (1996); Mishchenko and Travis (1998); Mishchenko (2000). We assume the drops to be oblate spheroids with axis ratios dependent on the drop diameters following the relationship of Thurai et al. (2007) and averaging over canting angles following a Gaussian distribution with a mean of 0° (vertical) and a standard deviation of 2°. Resulting scattering efficiencies at some relevant frequencies are shown in Fig. 2 as a function of volume-equivalent diameter.

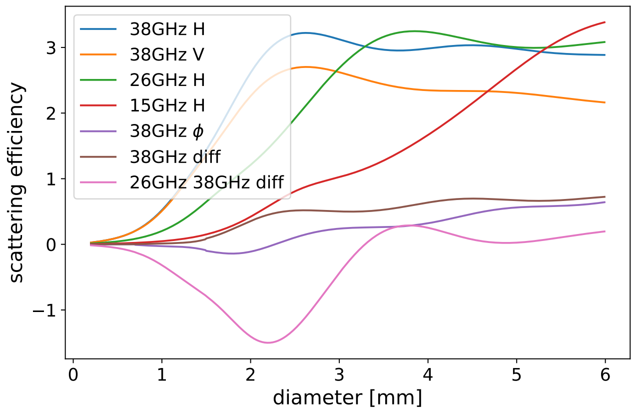

Figure 2. Scattering efficiency of raindrops as a function of drop volume-equivalent diameter modeled with the T-matrix method, at a temperature of 288 K.

The variables used as input in the retrieval could be attenuation of horizontally or vertically polarized radiation or phase differences between horizontally and vertically polarized radiation at one or several frequencies. In order to be able to use attenuations and phase differences interchangeably in the retrieval algorithm we rearrange Eqs (4), (5) and (7) to have the same form.

$$k^*_H = \int_0^\infty \sigma_H(D)N(D)dD \quad (11)$$

$$k^*_V = \int_0^\infty \sigma_V(D)N(D)dD \quad (12)$$

$$k^*_\phi = \int_0^\infty \sigma_\phi(D)N(D)dD, \quad (13)$$

where $k^*_H = k_H/C_k$, $k^*_V = k_V/C_k$, $k^*_\phi = \phi/C_\phi$, and the scattering cross-sections σ_X are the scattering efficiencies (Eqs (8)–(10)) multiplied by the drop cross-section ($\frac{1}{4}\pi D^2$): $\sigma_H = \frac{\lambda^2}{\pi}\Im[S_{HH}]$, $\sigma_V = \frac{\lambda^2}{\pi}\Im[S_{VV}]$ and $\sigma_\phi = \frac{\lambda^2}{\pi}\Re[S_{HH} - S_{VV}]$. We will from here on refer to an arbitrary input microwave link variable as k_i, where $i \in 1,2,3$, such that

$$k_i = \int_0^\infty \sigma_i(D)N(D)dD. \quad (14)$$

Atmos. Meas. Tech. Discuss., https://doi.org/10.5194/amt-2019-51
Manuscript under review for journal Atmos. Meas. Tech.
Discussion started: 17 April 2019

Atmospheric Measurement Techniques
Open Access
Discussions

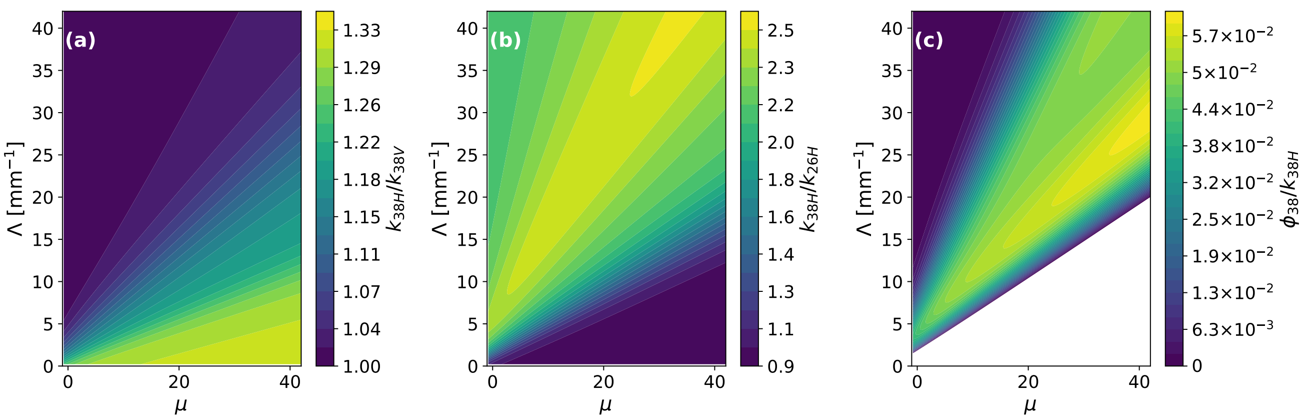

Figure 3. several ratios of microwave link observables that can be used as input to the DSD retrieval, as a function of parameters μ and Λ. a) k_{38H}/k_{38V}, b) k_{38H}/k_{26H} and c) ϕ_{38}/k_{38H}.

3.2 Three-parameter method

Inserting Eq. (1) into Eqs. (11) – (13) and taking the ratio of two variables we arrive at the following set of equations:

$$\begin{aligned} \frac{k1}{k2} &= \frac{\int_0^\infty \sigma_1(D) D^\mu e^{-\Lambda D} dD}{\int_0^\infty \sigma_2(D) D^\mu e^{-\Lambda D} dD} \\ \frac{k2}{k3} &= \frac{\int_0^\infty \sigma_2(D) D^\mu e^{-\Lambda D} dD}{\int_0^\infty \sigma_3(D) D^\mu e^{-\Lambda D} dD} \end{aligned} \tag{15}$$

Note that these ratios do not depend on the N_0 or N_T parameter. If we now replace the integrals by discrete summations we can use an iterative nonlinear root-finding technique to find values for μ and Λ from two ratios of microwave moments. Knowing μ and Λ, we can directly solve the discretized equation of one of the microwave link variables for N_T.

Fig. 3 shows several possible ratios of microwave link variables as a function of μ and Λ. These observables are calculated using the forward model of Eq. (15). Because it is possible to detect the attenuation of the horizontal signal and the vertical signal and the phase difference at a given frequency using a single set of antennae, we prefer this combination of variables over combinations of attenuations at multiple frequencies. We can see in Fig. 3 that the ratios k_H/k_V and ϕ/k_H provide complementary information and are therefore in principle suitable.

We use the Powell hybrid method to solve the system of equations of Eq. (15). We also tested several other gradient-based root-finding methods such as Levenberg-Marquardt and this makes little difference in the stability of the retrieval. The convergence of the retrieval is highly dependent on the initial guess. This is problematic, as we want to automatically retrieve a large number of DSDs without manual input. In many retrieval attempts the gradient-based root-finding algorithm diverges towards infinity. In order to prevent this we restrict the root finding algorithm to a limited range of parameter values. If the estimates reach the edge of the range, we reset the parameters to a new initial guess which is taken from within the allowed

Atmos. Meas. Tech. Discuss., https://doi.org/10.5194/amt-2019-51
Manuscript under review for journal Atmos. Meas. Tech.
Discussion started: 17 April 2019

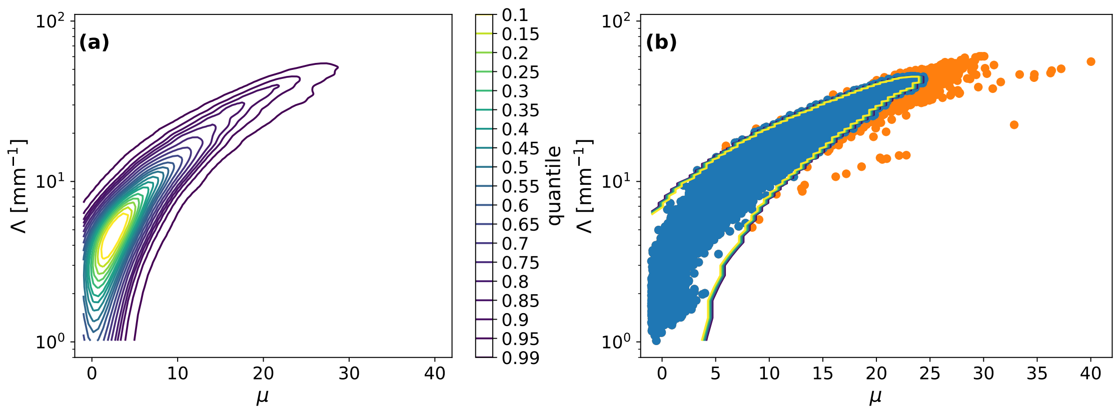

Figure 4. a) Density plot of gamma DSD parameter results from the method of moments, where density contours are given as quantiles enclosed within the contour. Results are for the complete 9-month set of path-averaged disdrometer data. b) 0.95 quantile contour overlaid on a scatterplot of all parameter combinations retrieved with the method of moments. Blue dots are inside the mask; Orange dots are outside the mask

range, but offset from the first guess by $\Delta\Lambda = 0.2\,\mathrm{mm}^{-1}$ or $\Delta\mu = 0.2$. We systematically traverse the μ-Λ space in this way starting from (-1, 0) until convergence is reached.

Even when the algorithm converges, the solution of the system of equations is not necessarily unique. We need an extra set of constraints to make sure we retrieve the parameters that are the most plausible. In order to do so we use the parameters retrieved by the analytical method of moments of Tokay and Short (1996) as a rough indication of plausible combinations of μ and Λ values. We have calculated the parameters using this method for all individual timesteps in the 9-month record of the spatially weighted average of the disdrometers placed in Wageningen. Figure 4b shows all these individual retrievals in the (Λ, μ) space. We then apply a kernel density estimator to this dataset (shown in Fig. 4a) and calculate the total fraction of data points contained within the contour lines. We then choose the contour corresponding to the 0.95 quantile as a mask. This mask is also shown in Fig. 4b.

The mask is then applied to all attenuation/phase-based numerical retrievals to define the range of allowed parameter values. If the estimate is outside this contour, we reset the root-finding algorithm with a new initial guess that is within the contour, but slightly perturbed from the previous initial guess as described above. This is continued until we find convergence within the contour or we reach the maximum number of iterations without a solution.

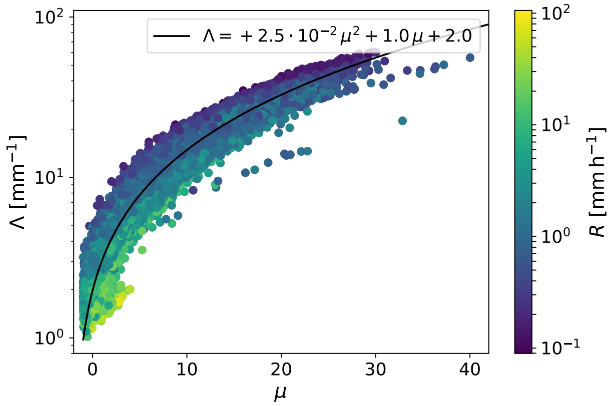

Figure 5. Polynomial fit of the Λ and μ parameters in the gamma distribution function fitted to parameter values obtained from the TS96 method of moments. based on the 9 months of path-averaged disdrometer data from Wageningen. The colors indicate the corresponding rain intensities.

3.3 Two-parameter method

When only two microwave link variables are available the system of equations of Eq. (15) is reduced to just one equation:

$$\frac{k1}{k2} = \frac{\int_0^\infty \sigma_1(D) D^\mu e^{-\Lambda D} dD}{\int_0^\infty \sigma_2(D) D^\mu e^{-\Lambda D} dD}. \tag{16}$$

In order to still solve for the two parameters an additional equation is required for the relationship between μ and Λ. We obtain this relationship empirically. We obtain gamma DSD parameter values via the analytical method of moments from the Wageningen disdrometer dataset. We then fit a second order polynomial function (as shown in Fig. 5) to the values of μ and Λ with a linear least-squares method. All 9 months of data were used to fit this function. The resulting relationship is

$$\Lambda = 2.5 \cdot 10^{-2}\mu^2 + 1.0\mu + 2.0, \tag{17}$$

which is similar in magnitude but still somewhat different to the relationship found by Zhang et al. (2003). We can substitute this equation for Λ in Eq. (16) and then solve for μ using Brent's root finding method. We prefer this method because it is not based on gradients and therefore guaranteed to find a solution if it exists. It is, however, not applicable to multivariate problems.

Figure 6 shows the ratio of Eq. (16) as a function of μ for two combinations of microwave attenuations that can be measured with the Wageningen link setup: two polarizations at 38 GHz and two frequencies (26 GHz and 38 GHz) at horizontal polarization. From this we can see that the dual polarization configuration is more suitable for retrieving the DSD; the dual frequency configuration has non-unique solutions for high underlying values of μ whereas the dual polarization model is monotonously decreasing over the entire range of valid μ values. On the other hand, the dual-frequency ratio of attenuations is much more

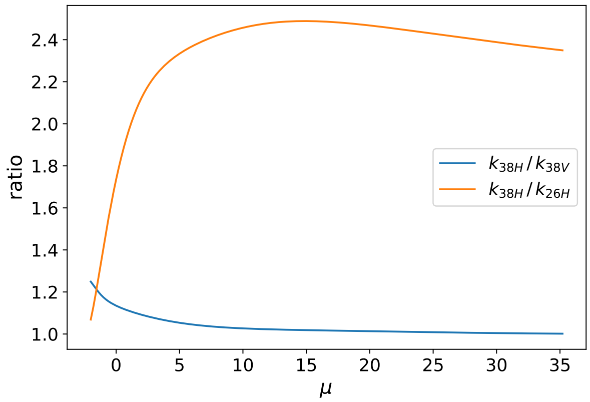

Figure 6. Ratios of attenuations as a function of the μ parameter for the two-parameter retrieval method.

sensitive to changes in μ for μ between -2 and 8, potentially yielding more accurate estimates of this parameter. For the dual-polarization ratio (at 38 GHz) it can also be seen that ratios lower than 1 and higher than 1.25 are not valid. If such ratios are observed they would yield no solution.

3.4 Validation methods

We test the capability of the methods to accurately retrieve DSDs and their associated statistical moments with two different datasets of measured drop size distributions. We use Eqs (11), (12) and (13) to calculate the microwave link variables from the known DSDs. We then use those variables as input to the retrieval algorithms described in the previous sections to retrieve the parameters of the gamma distribution approximating the DSD. From those parameters the complete DSD and its statistical moments are reconstructed. We then compare these to the original DSD and its moments to assess the systematic bias and random error in the retrieval. To be able to distinguish between cases where the gamma distribution is simply not a good fit for the measured DSD and cases where the retrieval itself is the cause for inaccuracies we also calculate the gamma parameters using the analytical method based on integer moments of DSD developed by Tokay and Short (1996) (TS96). These can be used to directly evaluate the parameters themselves as well if we assume the TS96 approach yields the correct parameters.

In order to assess the performance of the retrieval methods we will use a number of statistical measures throughout the results section. As a measure of the accuracy of the retrieval we use the median of the residuals (MOR). As a measure of the precision of the retrieval we use the median absolute deviation of the residuals with respect to the median of the residuals (MAD). We chose MAD and MOR over the use of standard deviation and means, because there are a relatively small number of extreme deviations which would otherwise have too much influence and thus would not give much information about the typical precision. The statistical metrics employed here are less influenced by non-normality and outliers. Because the number and severity of the extreme deviations is also an important part of the performance assessment of the retrieval, we also compute the 95th percentile absolute deviation with respect to the median of the residuals (95AD). Together with the MAD this gives a more complete picture of the distribution of the errors, while still being insensitive to the real outliers. All metrics are normalized with respect to the median of the original quantities.

4 Validation using simulated DSD

4.1 Single retrieval

Figure 7a shows a typical three-parameter retrieval result using horizontal attenuation, vertical attenuation and phase difference at a single frequency (38 GHz in this case). The normalized difference between the retrieved DSD and the original simulation procedure,

$$\Delta N^*(D) = \frac{N_r(D) - N_m(D)}{N_T}, \tag{18}$$

where N_r is the retrieved DSD, N_m is the originally measured DSD and N_T is the integral over all diameters of the original DSD, is illustrated in Fig. 7c. ΔN^* is within 10^{-4} for particles larger than 1 mm. However, at the smallest sizes the results tend to diverge up to $4.5 \cdot 10^{-3}$. In practice we are often more interested in quantities that scale with the statistical moments of the DSD rather than in the DSD itself. Important quantities are e.g. liquid water content W (3rd order moment), rain intensity R (close to 4th order) and radar reflectivity Z (6th order). For higher order moments, the contribution of the smallest drop sizes decreases. To illustrate this we also show the partial rain intensity as a function of drop diameter,

$$r(D) = \frac{\partial R(D)}{\partial D}, \tag{19}$$

for the same retrieval parameters in Fig. 7b. The normalized difference in the partial rain intensity (illustrated in Fig. 7d) is given by

$$\Delta r^*(D) = \frac{r_r(D) - r_o(D)}{R_o}, \tag{20}$$

where R_o is the total rain intensity based on the original DSD, $r_r(D)$ is the retrieved diameter-specific rain intensity and $r_o(D)$ is the original diameter-specific rain intensity. From Fig. 7d it can be seen that $-10^{-3} < \Delta r^* < 10^{-3}$ for all drop sizes. The difference in the total drop concentration is $\Delta N_T < 0.2 \cdot N_T$ in the first case, while the difference in the total rain intensity is $\Delta R < 0.03 \cdot R_o$. The assessment of the accuracy of such a retrieval must therefore take into account its most likely application. We will focus our attention in this section on the rainfall intensity and to a lesser extent on the individual gamma DSD parameters. In further sections, when more detailed comparison is required, we will also look at a range of integer moments.

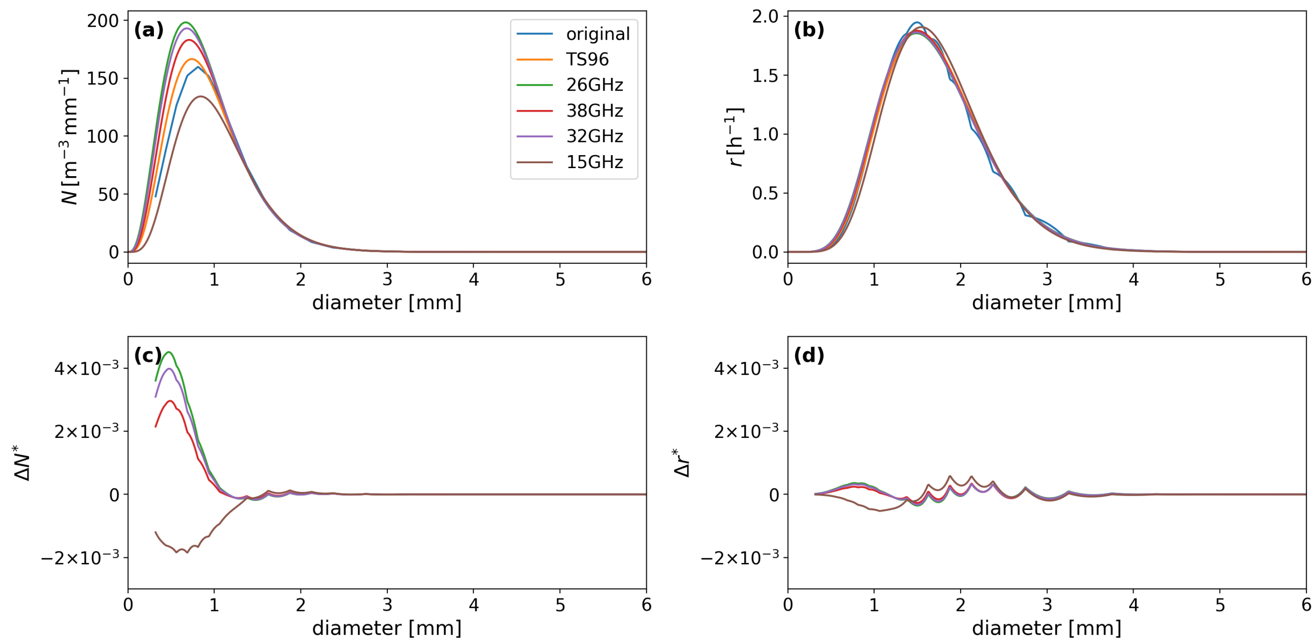

Figure 7. a) DSD retrieved from a single timestep in the first Ardèche event using several different microwave frequencies. b) Specific rain intensity for the same timstep. c) Relative difference in DSD compared to the original DSD. d) Relative difference in specific rain intensity compared to original DSD.

4.2 Complete events

Figure 8a shows the results of the 3-parameter retrieval for the first Ardèche event, which took place from 26 November 2012 at UTC 4:54 to 27 November at UTC 4:36. The total duration is almost 24 h and the precipitation intensity averages at 1.77 $\mathrm{mm\,h^{-1}}$ with a maximum of 10.29 $\mathrm{mm\,h^{-1}}$. The gamma DSD parameters of the retrieval are mostly very close to those of the direct method-of-moments procedure, with a few rather large exceptions, particularly noticeable in the N_T parameter. These outliers do not seem to correspond with any particularly high or low precipitation intensity. It can be seen that the temporal evolution of μ is very close to the temporal evolution of Λ, with a correlation coefficient of 0.86. Similar results can be observed for the second event (see Fig. 8b), which took place on 27 October 2013 from UTC 03:22 to UTC 8:48, with a total duration of 3.5 h, an average intensity of 1.58 $\mathrm{mm\,h^{-1}}$ and a maximum intensity of 27.05 $\mathrm{mm\,h^{-1}}$. The correlation coefficient between μ and Λ is $\rho = 0.87$.

Looking at the rainfall intensity over time for both events (Fig. 9a and c), we see that the retrieval not only corresponds closely with the analytical method-of-moments approach, but also with the rainfall intensity derived from the original DSD. There are only a handful of outliers here, the exact timing of which is dependent on the carrier frequencies for which the retrieval is attempted. The MOR, MAD and 95AD of the rain intensity is given in Table 1 for retrievals based on several

Atmos. Meas. Tech. Discuss., https://doi.org/10.5194/amt-2019-51
Manuscript under review for journal Atmos. Meas. Tech.
Discussion started: 17 April 2019

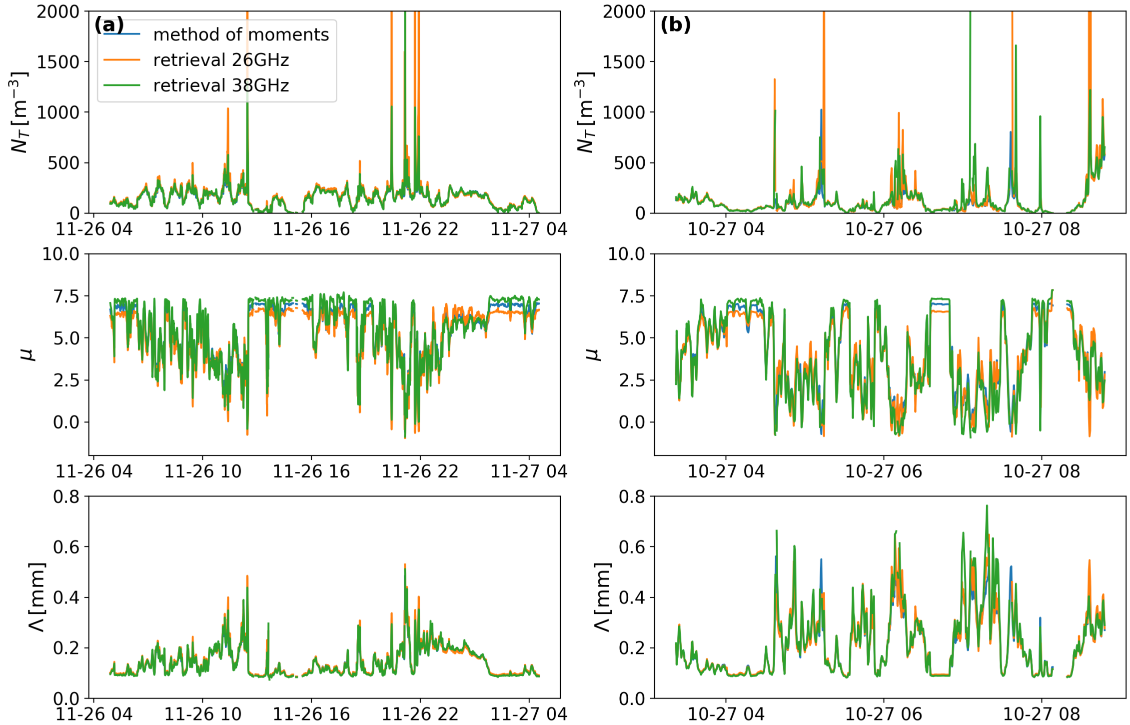

Figure 8. Gamma distribution parameters retrieved from the two simulated events from the Ardèche region on 26/27 November 2012 (a) and 27 October 2013 (b). The retrievals are performed using the three-parameter numerical microwave method and the TS96 method is shown as a reference.

different carrier frequencies. Another way of assessing the performance of the retrievals is to visualize the temporal mean of the DSD. This is shown in Fig. 9b and d. We can see that the retrieval gives an overestimation for small diameters (with the exception of very low carrier frequencies), while becoming more accurate for larger diameters. For diameters larger than 1 mm the residuals are lower than 0.1 $\mathrm{m^{-3}\,mm^{-1}}$.

5 Retrieval from disdrometers

We apply both the two-parameter and three-parameter retrieval algorithms to the Wageningen disdrometer dataset. The results are shown in Fig. 10. We selected a single rain event on 27 July 2015 starting at 9:40 UTC and ending at 12:00 UTC. The first notable difference between the Ardèche and the Wageningen datasets is that in the latter the values for μ and Λ are generally

Atmos. Meas. Tech. Discuss., https://doi.org/10.5194/amt-2019-51
Manuscript under review for journal Atmos. Meas. Tech.
Discussion started: 17 April 2019

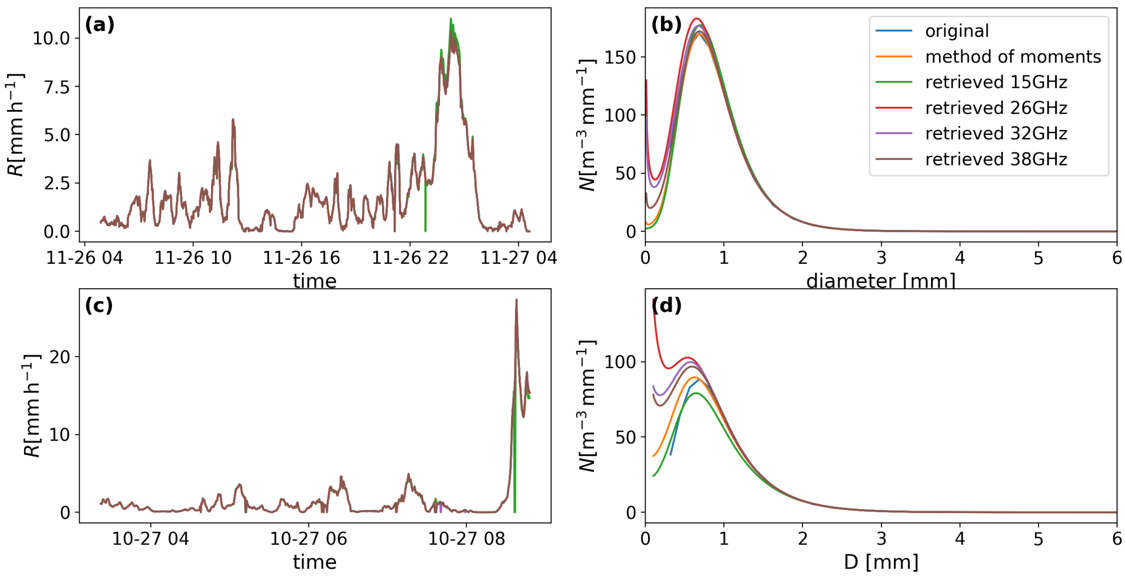

Figure 9. Rainfall intensity and mean drop size distribution retrieved on the basis of the two simulated events from the Ardèche region on 26/27 November 2012 (a) and 27 October 2013 (b). The retrievals are performed using the three-parameter method. The actual drop size distribution of the simulations and the DSD retrieved using the TS96 method is provided for comparison.

Table 1. Statistics of rainfall intensity R relevant to the accuracy and precision of the three-parameter retrieval for two simulated events from the Ardèche region. All statistics are normalized with respect to the median of the original rainfall intensity.

	15 GHz	26 GHz	32 GHz	38 GHz
Event 1 (mean: $1.77\,\mathrm{mm\,h^{-1}}$, median: $1.08\,\mathrm{mm\,h^{-1}}$)				
MOR	0.0048	0.0084	0.0068	0.0049
MAD	0.0037	0.0046	0.0042	0.0035
95AD	0.355	0.0202	0.0298	0.0362
Event 2 (mean: $1.58\,\mathrm{mm\,h^{-1}}$, median: $0.68\,\mathrm{mm\,h^{-1}}$)				
MOR	0.0017	0.0028	0.0045	0.0044
MAD	0.0065	0.0040	0.0037	0.0036
95AD	0.2304	0.0036	0.1197	0.0886

Table 2. Statistics of rainfall intensity R relevant to the accuracy and precision of the retrieval for 1 event and the whole dataset using the two parameter method based on the Wageningen disdrometer dataset. All statistics are normalized with respect to the median of the original measured rainfall intensity.

	15 GHz	26 GHz	32 GHz	38 GHz
Event 1 (mean: 7.81 $\mathrm{mm\,h^{-1}}$, median: 5.46 $\mathrm{mm\,h^{-1}}$)				
MOR	0.0000	0.0084	0.0081	0.0083
MAD	0.0176	0.0251	0.0220	0.0241
95AD	0.2533	0.1603	0.1486	0.2202
9 months (mean: 1.43 $\mathrm{mm\,h^{-1}}$, median: 0.69 $\mathrm{mm\,h^{-1}}$)				
MOR	0.0003	0.0003	0.0001	0.0001
MAD	0.0103	0.0167	0.0151	0.0141
95AD	0.3389	0.2523	0.2328	0.2473

much higher. For both the TS96 approach and the numerical retrieval, values higher than 20 occur regularly for both the μ and the Λ parameter, which is not consistent with what is typically found in the literature (e.g. Raupach and Berne (2016) for the Ardèche, Zhang et al. (2003) for Florida and Atlas and Ulbrich (2006) for Kapingamarangi Atoll (western tropical Pacific)). We can also see that in several timesteps the μ and Λ parameters in the retrieval are several times higher than they are in the TS96 method, but that this does not result in a significantly different rain intensity. Furthermore, when averaged over an entire event, the retrieval overestimates the number of drops with a diameter smaller than 1 mm and underestimates the number of drops with a diameter between 1 and 7.5 mm when compared to the measured DSD (except for very low carrier frequencies). The correlation between the method-of-moments derived μ and Λ parameters is very high at $\rho = 0.96$. The MOR, MAD and 95AD are given in Table 2. In general, the precision of the retrieval is an order of magnitude lower (higher MAD and 95AD), while the accuracy is actually higher (lower MOR) when compared with the Ardèche dataset.

5.1 Differences between two or three parameter retrievals

We summarize the differences in accuracy and precision between the two-parameter and the three-parameter method in Table 3. The analyses are all performed with respect to a 38-GHz dual-polarization retrieval (the third microwave link variable is the differential propagation phase). In addition, the number of failed retrievals (no solution at all) was 1.7 % higher when using only 2 moments. This indicates that there is at least some advantage to using 3 moments.

However, the differences in accuracy and precision of the retrieval between the three-parameter and two-parameter retrieval as measured by a range of integer moments is small and in many cases the two-parameter retrieval proved to be more reliable. Especially the number of sub-millimeter rain drops is severely overestimated by using the three-parameter method, as shown

Atmos. Meas. Tech. Discuss., https://doi.org/10.5194/amt-2019-51
Manuscript under review for journal Atmos. Meas. Tech.
Discussion started: 17 April 2019

Atmospheric Measurement Techniques
Discussions

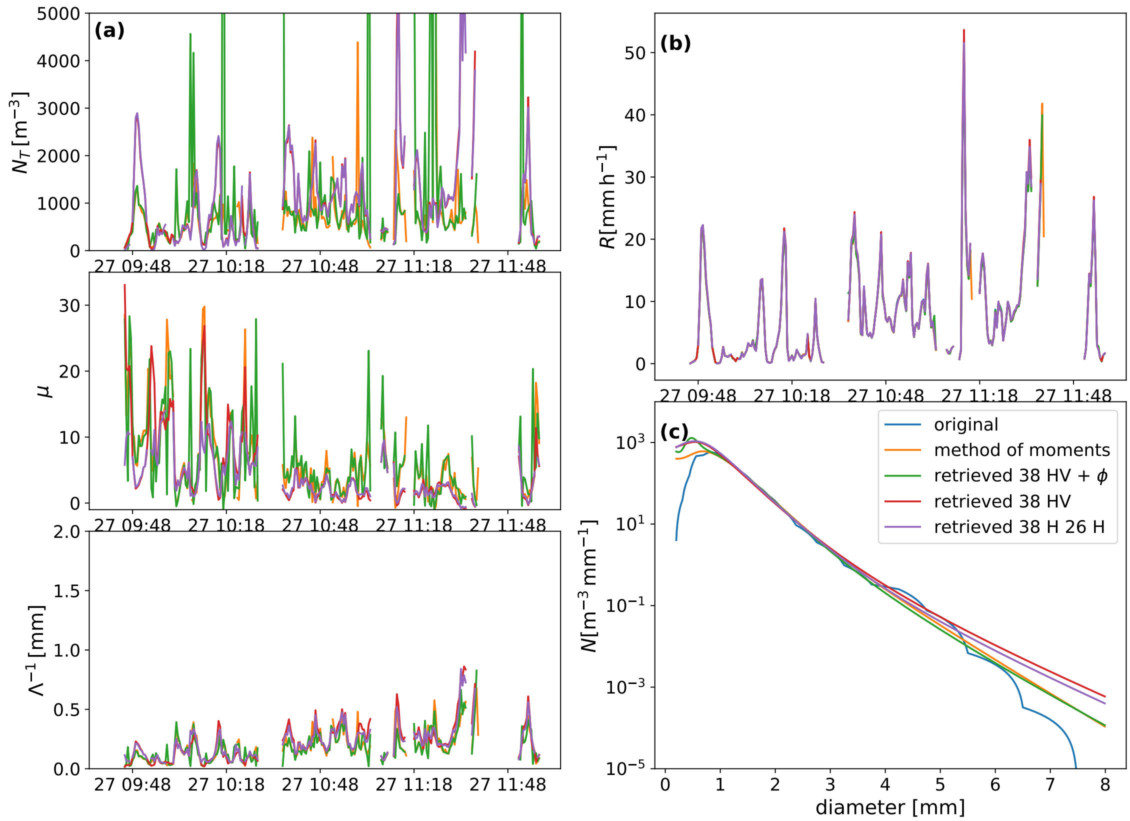

Figure 10. Retrieval of the event of 27 July 2015 using only the two attenuations at 38 GHz and a predetermined $\mu - \Lambda$ relation.

in Fig. 11. Therefore, the addition of a third microwave link variable does not improve the retrieval (in many cases it harms the retrieval) and is unnecessary. Aside from needing one less attenuation moment, the two-parameter retrieval is also orders of magnitude faster. This is because the numerical part is univariate and therefore the dimensionality of the problem is reduced and also more efficient root finding methods other than gradient-based methods can be used (such as Brent's method). We do not need the workaround for local minima either, which is computationally very inefficient.

Because these results show that a three-parameter retrieval provides little added value above a two-parameter retrieval and because the two-parameter retrievals are far less computationally intensive than three-parameter retrievals we will restrict ourselves to two-parameter retrievals in the remainder of this paper.

Atmos. Meas. Tech. Discuss., https://doi.org/10.5194/amt-2019-51
Manuscript under review for journal Atmos. Meas. Tech.
Discussion started: 17 April 2019

Table 3. Statistics of integer statistical moments M_i relevant to the accuracy and precision of the retrieval based on disdrometer data for all 9 months with both types of retrievals at 38 GHz. All statistics are normalized with respect to the median of the original measured moments.

	M0	M1	M2	M3	M4	M5	M6
Mean	197 m^{-3}	156 $mm\,m^{-3}$	144 $mm^2\,m^{-3}$	160 $mm^3\,m^{-3}$	220 $mm^4\,m^{-3}$	388 $mm^5\,m^{-3}$	905 $mm^6\,m^{-3}$
Median	128 m^{-3}	102 $mm\,m^{-3}$	91 $mm^2\,m^{-3}$	89 $mm^3\,m^{-3}$	97 $mm^4\,m^{-3}$	116 $mm^5\,m^{-3}$	152 $mm^6\,m^{-3}$
2 parameters							
MOR	0.0636	0.0176	-0.0009	-0.0029	0.0001	0.0013	0.0017
MAD	0.2462	0.1366	0.0691	0.0320	0.0132	0.084	0.0212
95AD	1.9254	1.1508	0.6625	0.3645	0.3653	1.1225	3.7447
3 parameters							
MOR	0.0321	0.0064	-0.0013	-0.0029	-0.0026	0.0007	0.0015
MAD	0.2855	0.1704	0.0922	0.0416	0.0133	0.00135	0.0339
95AD	4.4102	2.3506	1.2231	0.5870	0.2912	0.8814	2.8955

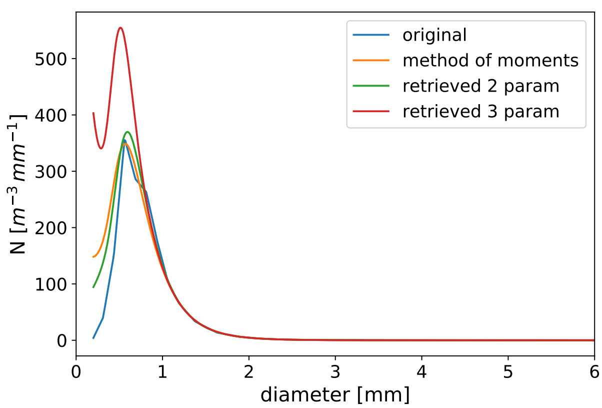

Figure 11. Mean over 9 months of DSD retrievals from simulated microwave link data based on disdrometer data from the Wageningen experiment using three methods: the analytical method of TS96, a numerical approach based on horizontal and vertical attenuation at 38 GHz (two-parameter retrieval) and a numerical approach including both attenuations and the phase difference at 38 GHz (three-parameter retrieval).

5.2 Dependence on link frequency

In order to determine the effect of the carrier frequencies of the links on the accuracy and precision of the retrieval we perform DSD retrievals at many different frequencies and calculate MOR, MAD and 95AD from the third order moment. We

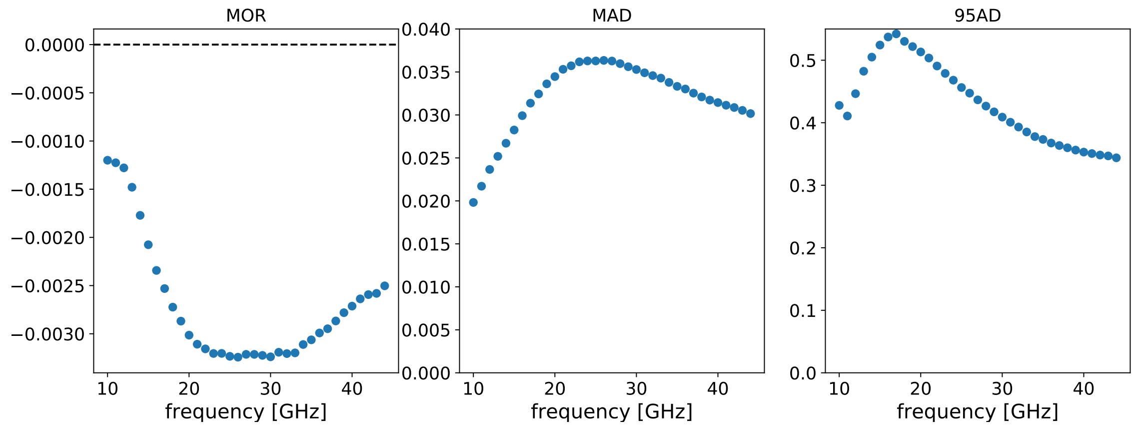

Figure 12. MOR, MAD and 95AD of the third order moment of the DSD estimated using a two-moment dual-pol retrieval as a function of carrier frequency based on disdrometer data. All statistics are normalized with respect to the median of the moment of the original measured DSD.

consider both dual polarization retrievals with frequencies ranging from 10 GHz to 45 GHz (with steps of 1 GHz) as well as dual frequency retrievals using every combination between 10 and 45 GHz. This range contains the bulk of microwave link frequencies found in typical communication networks. The results are shown for dual polarization in Fig. 12 and for dual frequency in Fig. 13. We can see in Fig. 12 that the accuracy and precision is high for all frequencies. However, the accuracy is pessimal for frequencies between 22 and 34 GHz. Similarly, MAD is largest around 25 GHz and 95AD is largest around 17 GHz. Therefore, for an optimal retrieval those intermediate frequencies should be avoided. Fig. 13 shows that the accuracy and precision of dual frequency retrievals is highest when both frequencies are high. The difference between the two frequencies does not seem to matter much; when the two frequencies are far apart the precision and frequency are actually slightly lower. Predictably, there are no solutions found when the frequencies are exactly the same. It should be noted that for this simulation, the effect of noise is not taken into account. It is expected that this would influence the retrieval the most when the frequencies are close together.

5.3 Sensitivity to attenuation bias

Because our retrieval algorithm uses ratios of attenuations as input, it is important that a reliable baseline power level is established from which to calculate the attenuations. To assess the sensitivity of the retrieval technique to inaccuracies in the baseline (dry) power level, we perform the two-moment retrievals based on the simulated attenuations from the disdrometer measurements but with an offset added to all input attenuations. Figure 14 shows the resulting DSDs averaged over 9 months for attenuation offsets between 0 and 5 dB and a path length of 2.2 km. For this analysis we chose two combinations of links that we will also later use for the actual link measurements: a dual polarization retrieval at 38 GHz and a dual frequency retrieval at 26 GHz and 38 GHz. We can see in Fig. 14a that the addition of an offset to the attenuation leads to an overestimation below 2

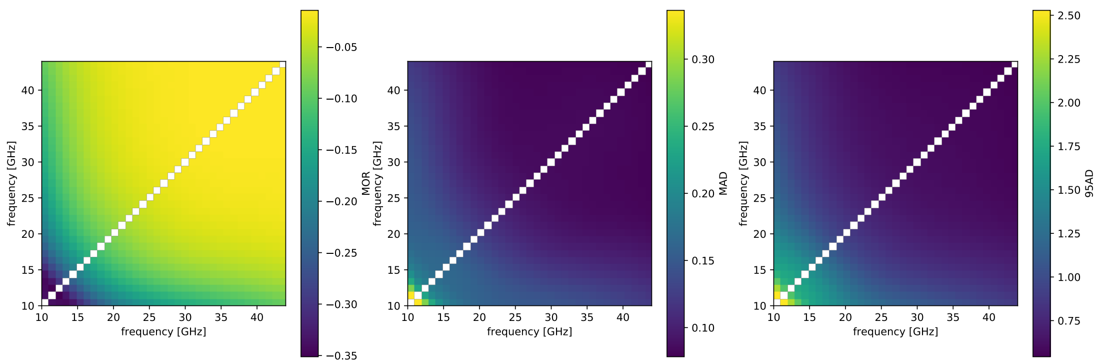

Figure 13. MOR, MAD and 95AD of the third order moment of the DSD estimated using a two-moment dual-frequency retrieval as a function of the two carrier frequencies based on disdrometer data. All statistics are normalized with respect to the median of the moment of the original measured DSD.

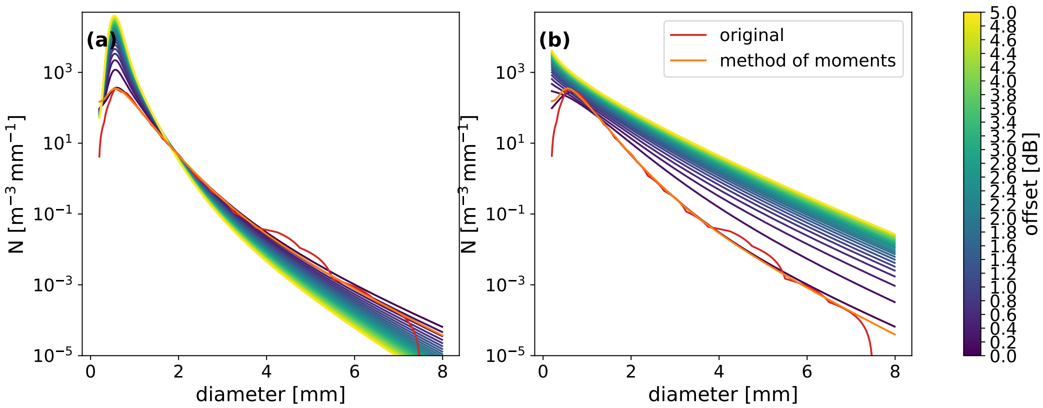

Figure 14. DSDs of the two-moment retrieval (38 GHz) of the 9-month Wageningen disdrometer dataset with an offset in the attenuations of 0 – 5 dB.

mm and an underestimation above 2 mm for the dual polarization retrieval. The introduction of an offset has no effect at 2 mm and the effects are largest below 1 mm. The effects for a dual frequency retrieval are quite different, as can be seen in Fig. 14b. There is an overestimation at all diameters. The overestimation is smallest around 1 mm and increasing towards higher and lower diameters. Overall, the mean bias is larger than for dual polarization retrievals and the shape of the DSD is especially sensitive to small offsets in the base power level.

Atmos. Meas. Tech. Discuss., https://doi.org/10.5194/amt-2019-51
Manuscript under review for journal Atmos. Meas. Tech.
Discussion started: 17 April 2019

6 Experimental link retrieval

Using the double-moment retrieval method we estimated the DSDs from actual link measurements of the Wageningen setup. The baseline power level of the links showed considerable fluctuations over the course of the measurement period. Therefore, it was not feasible to perform retrievals for the entire 9-month dataset. We selected the event of 27 July 2015 (see Fig. 15) because the power levels of the links in the period surrounding this event showed relatively little fluctuations. We determined a suitable constant baseline power level calibrated for this event. The measured attenuation after subtracting a baseline for this event is shown in Fig. 15 and compared with the path-average attenuation derived from the disdrometer measurements; The retrieval results are given in Fig. 16.

The resulting DSD is very similar in shape to that obtained in the simulations, with overestimations especially at smaller diameters but with the general shape of the DSD preserved. Closer inspection reveals that the bias and scatter compared to the original DSD are actually up to two orders of magnitude higher than in the simulations, as can be seen in Table 4. Nevertheless, at the important higher order moments related to e.g. liquid water content, rain rate, kinetic energy and radar reflectivity the bias is around 7 % for the dual-polarization retrieval. The scatter as indicated by the MAD is about one order of magnitude higher than the simulations across all moments. However, when taking the 95AD as measure of scatter, the order of magnitude is the same. There are a few more intervals with no solution at all when compared to the simulations. These correspond with ratios of observables that are outside the range of the forward model (see Fig. 6). The ratios for the dual polarization retrieval are illustrated in Fig. 15b. These intervals with extremely low or high ratios between attenuations mostly (but not always) occur when the rain intensity is low and thus other sources of signal variability are more dominant. Overall the dual polarization and dual frequency retrievals have a similar performance in this case. However, using two frequencies instead of two polarizations leads to a higher accuracy for low order moments (up to 4th), but lower accuracy for higher order moments. No plausible solutions for the retrieval where obtained when using the phase difference instead of one of the attenuations or with a triple variable retrieval. Very few intervals led to convergence at all with this configuration.

7 Discussion

7.1 Feasibility in practice

Constraints on the feasibility of this method in practice fall into three broad categories: availability of multiple link signals on the same path; quality of the available signals; and real-time processing speed.

The use of a three-moment retrieval means that three moments on the same path need to be available. This is rare in commercial networks; Therefore this method is most readily applicable to dedicated research networks. There are several different combinations of moments to choose from. However, in our approach we focused on the combination of a horizontal attenuation, vertical attenuation and phase difference at the same carrier frequency. This allows the use of a single set of antennae for all three moments, allowing for the use of a more compact and less expensive device (such as the device that was used in this test setup).

Atmos. Meas. Tech. Discuss., https://doi.org/10.5194/amt-2019-51
Manuscript under review for journal Atmos. Meas. Tech.
Discussion started: 17 April 2019

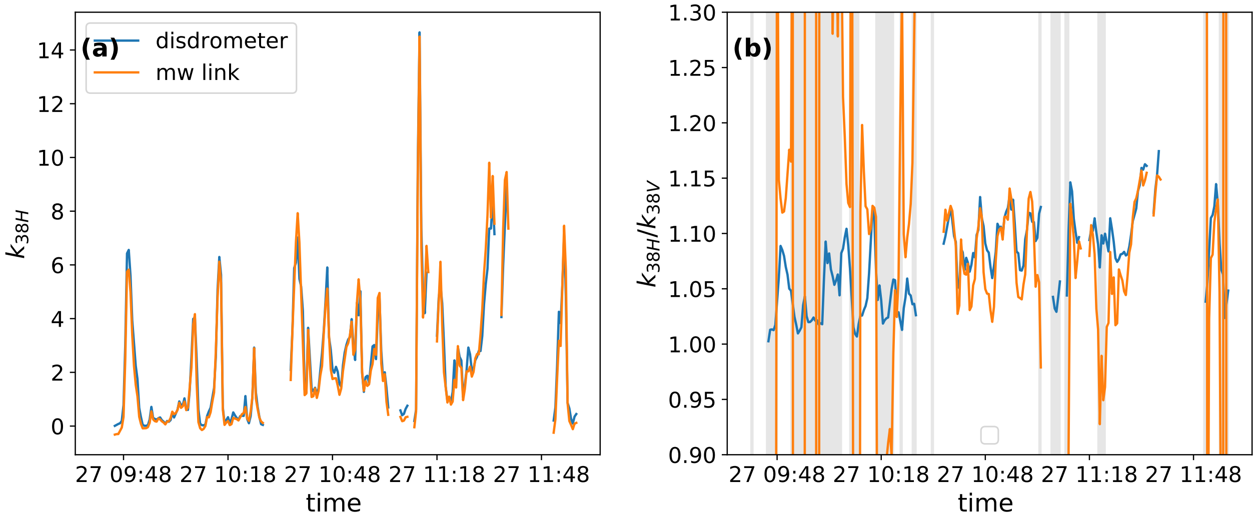

Figure 15. a) Link attenuation at 38GHz with vertical polarization. Time series are shown for link measurements (orange) as well as attenuation computed from disdrometer data (blue) for the event of 27 July 2015. b) Ratios of the attenuations of the horizontally and vertically polarized signal, from link and disdrometer data. Shaded areas indicate intervals where the ratio is outside of the solvable range for the dual polarization retrieval (1.00 – 1.25; see Fig. (6)).

Table 4. Statistics of accuracy and precision of the retrieval of integer moments of the DSD for the event of 27 July 2015 using actual link data from two different combinations of links. All statistics are normalized with respect to the median of the moments of the disdrometer data.

	M0	M1	M2	M3	M4	M5	M6
Mean	584 m^{-3}	615 mm m^{-3}	758 mm^2 m^{-3}	1102 mm^3 m^{-3}	1923 mm^4 m^{-3}	4109 mm^5 m^{-3}	10868 mm^6 m^{-3}
Median	548 m^{-3}	573 mm m^{-3}	694 mm^2 m^{-3}	951 mm^3 m^{-3}	1479 mm^4 m^{-3}	2790 mm^5 m^{-3}	5934 mm^6 m^{-3}
38 GHz H, V							
MOR	1.2827	0.6175	0.2846	0.0688	-0.0074	-0.0678	-0.0739
MAD	0.4937	0.3190	0.2033	0.1194	0.1152	0.2715	0.4757
95AD	2.1555	1.4571	0.8718	0.5390	0.7271	1.4348	2.9816
26 GHz H, 38 GHz H							
MOR	0.6793	0.2007	0.0177	-0.353	0.0014	0.0968	0.1915
MAD	0.9755	0.5562	0.3324	0.1536	0.1284	0.2632	0.5718
95AD	2.4556	1.6023	1.0235	0.7045	0.5414	1.4086	3.2212

Atmos. Meas. Tech. Discuss., https://doi.org/10.5194/amt-2019-51
Manuscript under review for journal Atmos. Meas. Tech.
Discussion started: 17 April 2019

Atmospheric Measurement Techniques
Open Access
Discussions

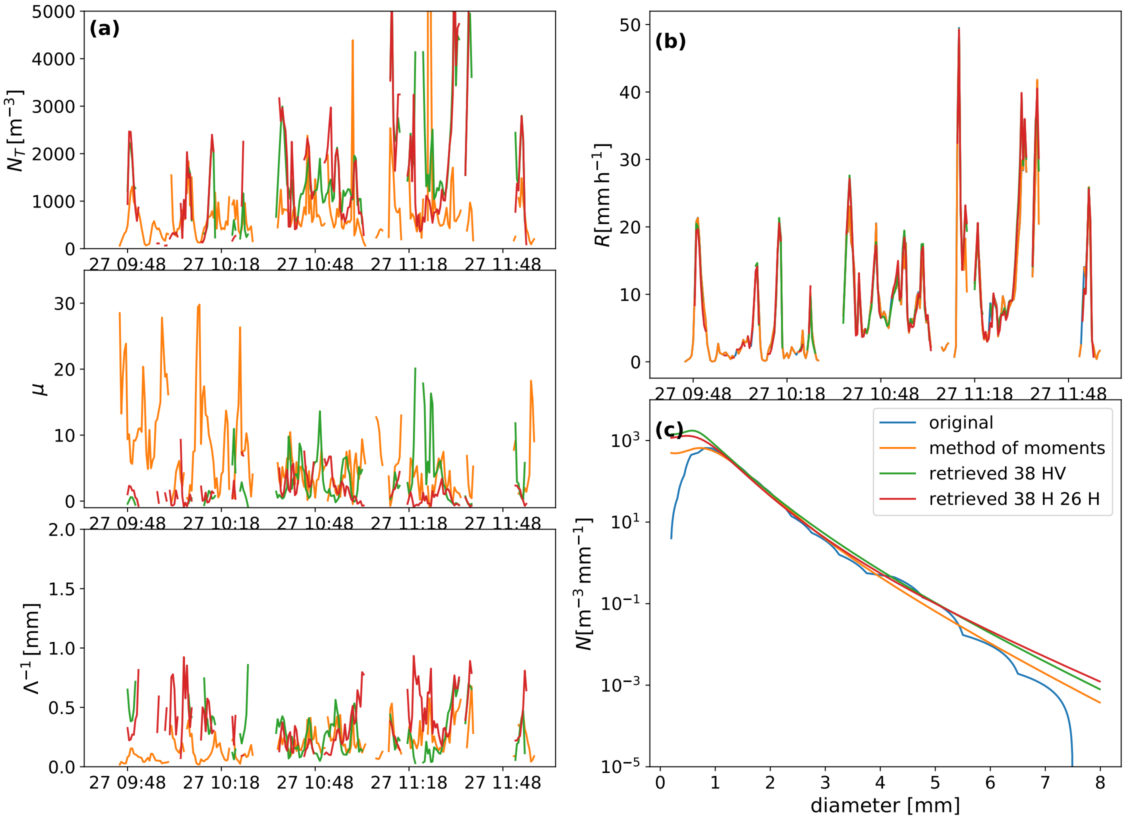

Figure 16. Retrieval results for the event of 27 July as measured by the 38 GHz instrument using horizontal and vertical polarization and the 26 GHz instrument using horizontal polarization. The method of moments results are derived from the five disdrometers for the same event.

The second concern is with regard to the quality and reliability of the signal. In order to apply the method in practice it is essential that a baseline (no rain) signal is accurately determined. because the method relies on the ratios of attenuations, small deviations in the baseline determination can result in large deviations in the retrieval (and even non-convergence). No such problem exists in principle with regard to the phase difference; It is independent of any baseline as long as that baseline is indifferent to polarization. However, phase difference on its own is not sufficient for the retrieval. To have a chance at a successful retrieval the baseline needs to be as invariant as possible. Where it is not, the variability should be accurately modeled and predicted from auxiliary measurements. In our own preliminary attempts we found our instruments lacking in stability. In particular the clinging of drops to the antenna cover (as described in van Leth et al., 2018) seems an intractable problem. However, as was also described in that paper, we found that a former commercial microwave link had a much stabler baseline and furthermore the effect of wet antennas was much more manageable for that particular device. This provides a hopeful perspective for the application of this method to commercial networks.

The third constraint is only relevant when real-time processing is required. The three-moment method is relatively wasteful with computing cycles because of the repeated reinitialization of the root finding process. We might expect this to become a bottleneck. However, in its current implementation the processing of 9 months of data from one link requires roughly three hours of wall time on a high-end desktop workstation. This is while utilizing 10 CPU cores simultaneously. Such a setup is therefore expected to be able to process a network of more than 2000 links in real-time. Nevertheless, reducing this computational load would make real-time retrievals more feasible on low-end (embedded) hardware as well. We already found that the specific programmatic implementation of the root-finding algorithm can make an order of magnitude difference in computation time. The use of pre-computed lookup tables may help to bring down computation time in a real-time setting. The two-moment method requires far less computation (e.g. processing the same 9 months of data with the same workstation requires only 5 minutes), which makes it far more suitable for real-time processing.

7.2 Caveats

There are a number of caveats to our methods which could influence the interpretation of the results: Firstly, we use a threshold of 50 drops per disdrometer to filter out low quality measurements before calculating the mask or μ-Λ fit. How high this number should be is debatable (e.g. Uijlenhoet et al. (2006)). A threshold that is too low might allow for many erroneous measurements that are not representative of rain. On the other hand, a threshold that is too high might result in too many reasonable measurements being rejected. This might mean the results are less statistically representative and possibly biased towards high rain intensities. The number used here is therefore a compromise and the resulting relationships do change somewhat depending on the threshold chosen. A similar consideration applies to the choice too filter on a per-instrument basis instead of on the basis of the total drop count. Filtering on a per-instrument basis makes it more likely that all instruments where measuring correctly. However, it does bias the measurements towards more homogeneous rainfall. Considering the small spatial scale of the measurements we considered and the high spatial correlations therein this is an acceptable loss.

Another consideration is the use of the mask itself. The mask is determined on the basis of the measured disdrometer data. We then use this mask in, among others, the retrieval of the DSD from the disdrometer-derived simulated variables. There is

Atmos. Meas. Tech. Discuss., https://doi.org/10.5194/amt-2019-51
Manuscript under review for journal Atmos. Meas. Tech.
Discussion started: 17 April 2019

certainly something circular about this. Nevertheless, this data is never used as input for the root-finding procedure itself. It is only used a posteriori to assess whether the results fall into a plausible range of values. Potentially more serious is the use of the predetermined μ-Λ relationship in the case of the two-parameter retrieval. In this case, the relationship determined on the basis of the disdrometer measurements is used more directly in the retrieval. This might have colored the results somewhat in favor of the two-parameter retrieval as opposed to the three-parameter retrieval. Somewhat alleviating is the fact that both the μ-Λ relationship and the mask are determined from the total of all 9 months of disdrometer measurements, not from the specific event in question.

The third consideration is the underlying assumption that the untruncated gamma distribution is applicable throughout the diameter domain. It is on the basis of this assumption that we treat the values of μ and Λ derived from the TS96 method of moments as the correct parameter values. The gamma distribution has a non-zero value up to positive infinity. Meanwhile, there are both physical and instrumental cutoffs to the maximum drop size that can occur. This would suggest that a truncation should be included in the expression of the gamma distribution. However, the truncation of the gamma distribution at high diameters is not relevant in this case because we can see in Figs. 7a, 9b and d, 10c, 11 and 16c that the gamma distribution corresponding to the DSDs under consideration tends to zero (or $< 10^{-2}\mathrm{m}^{-3}\,\mathrm{mm}^{-1}$) before the instrumental cutoff. We can also observe from those figures that the systematic deviation between the measured (interpolated) DSD and the DSD obtained from the method of moments is small. Instrumental cutoff at the small end of the diameter scale is relevant in this case, but the effects of this on higher order moments is minute. Regardless, since the attenuation/phase based retrieval in this case is limited to three parameters, it is not possible to include a cutoff there. A retrieval using even more signals might make this possible, but this would further limit the practical applicability of this method.

8 Conclusions and outlook

Using both simulations and actual link data we have shown that a DSD retrieval on the basis of multiple microwave link variables can be successful and highly accurate. Both the use of dual-polarization and dual-frequency retrievals is feasible. However, the use of dual-polarization is less sensitive to inaccuracies in the base power level than the use of dual-frequency links. Simulated retrievals using a variety of frequencies show that, at least between 10 GHz and 45 GHz, the accuracy and precision of the retrievals is very high for all frequency combinations. Therefore, the frequency chosen for a dual polarization retrieval is not very important. Nevertheless, when a choice is available, our simulations indicate that frequencies at the lowest end or the highest end of the range are preferred. Furthermore, at the lowest end of the frequency range there is less attenuation in general and therefore a smaller difference in attenuation. This could more easily be obscured by noise or quantization effect. Therefore, the higher end of the tested frequencies are optimal. For dual frequency retrievals, bias and random error are an order of magnitude higher than for the dual polarization retrievals. If a dual frequency retrieval is attempted, both frequencies should be as high as possible to minimize the bias and random error. Curiously, in our simulation, retrievals performed using two frequencies 1 or 2 GHz apart were just as accurate as retrievals using two frequencies that are further apart. However, it is expected that this would change if noise is taken into account.

In our field experiment we tested a dual-frequency retrieval using 26 GHz and 38 GHz as well as a dual polarization retrieval at 38 GHz. Both retrievals produced good results for a selected summer event where other attenuating atmospheric phenomena where not present. The feasibility of the retrieval does however depend very much on a stable base power level, which was not guaranteed in our experiment. The Nokia link (former commercial link) is promising in this respect, because it was much stabler and less sensitive to e.g. temperature fluctuations and antenna wetting.

Using phase differences in addition to attenuations is feasible in the simulations. However, in practice these measurements are not accurate enough to yield meaningful solutions. In most instances no convergence was obtained. We have also shown that using three microwave link variables yields no improvements over a retrieval using only two variables, which is also computationally faster and more readily applicable in operational settings. At least in comparable climatologies to those treated here, a predetermined μ-Λ relation suffices to determine the gamma DSD parameters from two attenuations.

A follow-up experiment using different microwave links of similar frequencies (preferably commercially available ones) is needed to determine if the base power level of commercial links is sufficiently stable for reliable continuous observations. A tally should also be done on the number of dual polarized links in cellular communications networks to determine if it is feasible to retrieve spatial DSD information from such networks or whether this technique is only applicable to some individual link paths, either from commercial or research networks. Another concern is the quantization of data from commercial link networks. As the difference between the attenuation of the horizontal signal and the vertical signal is often a fraction of a dB and data available from such networks are often rounded to 0.1, 0.5 or 1 dB, this might limit the applicability of this method. Therefore, the possibility of collecting higher resolution data from such instruments should be looked into.

Acknowledgements. The Ardèche dataset was kindly provided by Timothy H. Raupach. Funding was provided by NWO-TTW (project number 11944).

References

Angulo-Martínez, M. and Barros, A.: Measurement uncertainty in rainfall kinetic energy and intensity relationships for soil erosion studies: An evaluation using PARSIVEL disdrometers in the southern Appalachian mountains, Geomorphology, 228, 28–40, doi:10.1016/j.geomorph.2014.07.036, 2015.

Atlas, D. and Ulbrich, C. W.: Drop size spectra and integral remote sensing parameters in the transition from convective to stratiform rain, Geophysical Research Letters, 33, doi:10.1029/2006GL026824, 2006.

Cao, Q., Zhang, G., Brandes, E. A., and Schuur, T. J.: Polarimetric radar rain estimation through retrieval of drop size distribution using a Bayesian approach, Journal of Applied Meteorology and Climatology, 49, 973–990, doi:10.1175/2009JAMC2227.1, 2010.

Cherkassky, D., Ostrometzky, J., and Messer, H.: Precipitation classification using measurements from commercial microwave links, IEEE Transactions on Geoscience and Remote Sensing, 52, 2350–2356, 2014.

David, N., Alpert, P., and Messer, H.: The potential of commercial microwave networks to monitor dense fog-feasibility study, Journal of Geophysical Research: Atmospheres, 118, 750–761, 2013.

De Vos, L. W., Raupach, T. H., Leijnse, H., Overeem, A., Berne, A., and Uijlenhoet, R.: High-resolution simulation study exploring the potential of radars, crowdsourced personal weather stations, and commercial microwave links to monitor small-scale urban rainfall, Water Resources Research, 54, doi:10.1029/2018WR023393, 2018.

Fabry, F.: The added value of dual polarization, in: Radar Meteorology: Principles and Practice, pp. 92–114, Cambridge University Press, doi:10.1017/CBO97811077074505.007, 2015.

Gorgucci, E., Chandrasekar, V., Bringi, V. N., and Scarchilli, G.: Estimation of raindrop size distribution parameters from polarimetric radar measurements, Journal of Atmospheric Sciences, 59, 2373–2384, 2002.

Gosset, M., Kunstmann, H., Zougmore, F., Cazenave, F., Leijnse, H., Uijlenhoet, R., Chwala, C., keis, F., Doumounia, A., Boubacar, B., Kacou, M., alpert, P., Messer, H., Rieckermann, J., and Hoedjes, J.: Improving rainfall measurement in gauge poor regions thanks to mobile telecommunication networks, Bull. Amer. Meteor. Soc., 97, ES49–ES51, doi:10.1175/BAMS-D-15-00164.1, 2016.

Hazenberg, P., leijnse, H., and remko Uijlenhoet: The impact of reflectivity correction and accounting for raindrop size distribution variability to imrpove precipitation estimation by weather radar for an extreme low-land mesoscale convective system, Journal of Hydrology, 519, 3410–3425, doi:10.1016/j.hydrol.2014.09.057, 2014.

Islam, T., Rico-Ramirez, M. A., and Han, D.: Tree-based genetic programming approach to infer microphysical paramters of the DSDs from the polarization diversity measurements, Computers and Geosciences, 48, 20–30, doi:10.1016/j.cageo.2012.05.028, 2012.

Leijnse, H., Uijlenhoet, R., and Stricker, J.: Hydrometeorological application of a microwave link: 1. Evaporation, Water Resources Research, 43, 2007a.

Leijnse, H., Uijlenhoet, R., and Stricker, J.: Rainfall measurement using radio links from cellular communication networks, Water Resources Research, 43, 2007b.

Messer, H., Zinevich, A., and Alpert, P.: Environmental monitoring by wireless communication networks, Science, 312, 713, 2006.

Mishchenko, M. I.: Calculation of the amplitude matrix for a nonspherical particle in a fixed orientation, Applied Optics, 39, 1026–1031, 2000.

Mishchenko, M. I. and Travis, L. D.: Capabilities and limitations of a current FORTRAN implementation of the T-matrix method for randomly oriented, rotationally symmetric scatterers, Journal of Quantitative Spectroscopy and Radiative Transfer, 60, 309–324, 1998.

Atmos. Meas. Tech. Discuss., https://doi.org/10.5194/amt-2019-51
Manuscript under review for journal Atmos. Meas. Tech.
Discussion started: 17 April 2019

Atmospheric Measurement Techniques
Discussions

Mishchenko, M. I., Travis, L. D., and Mackowski, D. W.: T-matrix computations of light scattering by nonspherical particles: a review, Journal of Quantitative Spectroscopy and Radiative Transfer, 55, 535–575, 1996.

Raupach, T. H. and Berne, A.: Correction of raindrop size distributions measured by Parsivel disdrometers, using a two-dimensional video disdrometer as a reference, Atmospheric Measurement Techniques, 8, 343–365, 2015.

Raupach, T. H. and Berne, A.: Spatial interpolation of experimental raindrop size distribution spectra, Quarterly Journal of the Royal Meteorological Society, 142, 125–137, 2016.

Raupach, T. H. and Berne, A.: Retrieval of the raindrop size distribution from polarimetric radar data using double-moment normalization, Atmospheric Measurement Techniques, 10, 2573–2594, doi:10.5194/amt-10-2573-2017, 2017.

Rincon, R. F. and Lang, R. H.: Microwave link dual-wavelength measurements of path-average attenuation for the estimation of drop size distributions and rainfall, IEEE Transactions on Geoscience and Remote Sensing, 40, 760–770, 2002.

Salles, C. and Poesen, J.: Performance of an optical spesctro pluviometer in measuring basic rain erosivity characteristics, Journal of Hydrology, 218, 142–156, doi:10.1016/S0022-1694(99)00031-1, 1999.

Salles, C. and Poesen, J.: Rain properties controlling soil splash detachment, Hydrological Processes, 2000.

Salles, C., Poesen, J., and Borselli, L.: Measurement of simulated drop size distribution with an optical spectro pluviometer: Sample size considerations, Earth Surface Processes and Landforms, 24, 545–556, doi:10.1002/(SICI)1096-9837(199906)24:6<545::AID-ESP3>3.0.CO;2-D, 1999.

Thurai, M., Huang, G., Bringi, V., Randeu, W., and Schönhuber, M.: Drop shapes, model comparisons, and calculations of polarimetric radar parameters in rain, Journal of Atmospheric and Oceanic Technology, 24, 1019–1032, 2007.

Tokay, A. and Short, D. A.: Evidence from tropical raindrop spectra of the origin of rain from stratiform versus convective clouds, Journal of Applied Meteorology, 35, 355–371, 1996.

Uijlenhoet, R. and Stricker, J.: A consistent rainfall parameterization based on the exponential raindrop size distribution, Journal of Hydrology, 218, 101–127, doi:10.1016/S0022-1694(99)00032-3, 1999.

Uijlenhoet, R., Smith, J. A., and Steiner, M.: The microphysical structure of extreme precipitation as inferred from ground-based raindrop spectra, Journal of the Atmospheric Sciences, 60, 1220–1238, doi:10.1175/1520-0469(2003)60<1220:TMSOEP>2.0.CO;2, 2003.

Uijlenhoet, R., Porrà, J. M., Sempere Torres, D., and Creutin, J.-D.: Analytical solutions to sampling effects in drop size distribution measurements during stationary rainfall: Estimation of bulk rainfall variables, Journal of Hydrology, 2006.

Ulbrich, C. W.: Natural variations in the analytical form of the raindrop size distribution, Journal of Climate and Applied Meteorology, 22, 1764–1775, 1983.

Van Leth, T. C., Overeem, A., Leijnse, H., and Uijlenhoet, R.: A measurement campaign to assess sources of error in microwave link rainfall estimation, Atmospheric Measurement Techniques, 11, 4645–4669, 2018.

Vulpiani, G., Marzano, F. S., Chandrasekar, V., Berne, A., and Uijlenhoet, R.: Polarimetric weather radar retrieval of raindrop size distribution by means of a regularized artificial neural network, IEEE Transactions on Geoscience and Remote Sensing, 44, 3262–3275, 2006.

Waterman, P.: Matrix Formulation of Electromagnetic Scattering, Proceedings of the IEEE, 53, 805–812, 1965.

Zhang, G., Vivekanandan, J., and Brandes, E.: A method for estimating rain rate and drop size distribution from polarimetric radar measurements, IEEE Transactions on Geoscience and Remote Sensing, 39, 830–841, 2001.

Zhang, G., Vivekanandan, J., Brandes, E. A., Meneghini, R., and Kozu, T.: The shape-slope relation in observed gamma raindrop size distributions: statistical error of useful information?, 20, 1106–1119, 2003.